Reports

Possible Evidence for Superconducting Layers in Single Crystal $YBa_2Cu_3O_{7-x}$ by Field Ion Microscopy

A. J. MELMED, R. D. SHULL, C. K. CHIANG, H. A. FOWLER

The high-transition-temperature superconducting ceramic material $YBa_2Cu_3O_{7-x}$ ($0 < x < 0.5$) has been examined by field ion microscopy. Specimens from nominally superconducting and nonsuperconducting samples (determined by magnetic susceptibility measurements) were studied by field ion microscopy and significant differences were found. Preferential imaging of atomic or molecular layers, due to preferential field evaporation, field ionization, or both, was found in the superconducting phase below the transition temperature and is interpreted as possible evidence for the occurrence of relatively highly conducting layers in the $YBa_2Cu_3O_{7-x}$ unit cell perpendicular to the orthorhombic *c*-axis. Similar results were obtained for $YbBa_2Cu_3O_{7-x}$.

THE RECENTLY DISCOVERED HIGH-transition-temperature superconducting ceramic materials (*1*) present a challenge to the various high-resolution microscopies. Field ion microscopy (FIM) can be used for the real space observation of the qualitative atomic structure of materials (*2*), but FIM ordinarily might be considered unlikely to provide any information about these new superconducting materials, because of their complex structure that contains four different kinds of atoms and includes a large percentage of oxygen. However, we have imaged some of these materials by FIM and have found atomic striations in the images that may be due to preferentially conducting layers in the material.

Electron microscopy of the superconductor $YBa_2Cu_3O_{7-x}$ ($0 < x < 0.5$) has shown (*3*) that the specimens studied consisted of a mixture of at least two phases: an orthorhombic phase with many twins, which is believed to be responsible for the superconducting properties, and a closely related tetragonal phase.

X-ray and neutron diffraction studies have shown that the superconducting oxide $YBa_2Cu_3O_{7-x}$ is orthorhombic with the space group *Pmmm* (*4–6*). Replacement of the yttrium atom (*7–9*), which is located at the unit cell center, by other rare earth atoms does not change the superconducting transition temperature (T_c) of the material, despite the large magnetic moments possessed by some of these replacement atoms. This suggests that the superconductivity in high T_c oxides is localized in parts of the unit cell remote from the central rare earth atom. Furthermore, the only difference between the nonsuperconducting oxygen-deficient material $YBa_2Cu_3O_6$ (*10*) and the superconducting form of the oxide is the presence in the superconducting material of Cu-O-Cu chains along the *b*-axis direction in the atomic layers at either end of the unit cell. Such a localization of superconductivity would certainly lead to an anisotropy in the electrical properties, as experimentally found in the electrical resistivity (*11*), critical currents (*12*), and critical fields (*13*).

Two types of material were used in the present work: "as prepared" (by conventional methods) (*4*) $YBa_2Cu_3O_{7-x}$ and the oxygen-depleted $YBa_2Cu_3O_6$. The latter material was prepared by a subsequent heat treatment (*10*) of the "as prepared" $YBa_2Cu_3O_{7-x}$ for 10 hours at 870°C in nitrogen. Low alternating field (~0.5 gauss) magnetic susceptibility measurements as a function of temperature were made for both of these materials with a Hartshorn-type bridge circuit (Fig. 1). These results showed that the "as prepared" $YBa_2Cu_3O_{7-x}$ contained a high percentage of superconducting material with a T_c of 92 K and that the nitrogen-treated specimen was essentially nonsuperconducting down to 6 K.

We did not attempt to use conventional methods of FIM specimen preparation because we believe that chemical, electrochemical, and ion beam milling procedures could introduce artifacts into this already compli-

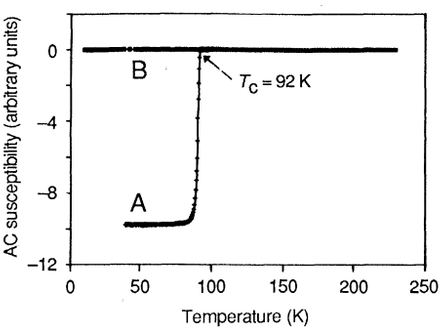

Fig. 1. Plot of ac magnetic susceptibility versus temperature for $YBa_2Cu_3O_{7-x}$ for the (A) "as prepared" and (B) oxygen-depleted conditions. A value of −10 on the *y*-axis indicates complete diamagnetism.

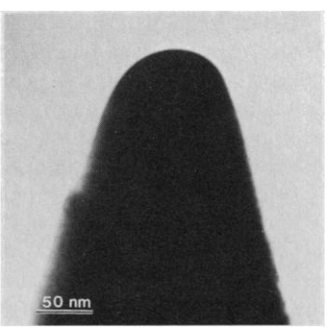

Fig. 2. Transmission electron microscopy of a random $YBa_2Cu_3O_{7-x}$ FIM specimen after field evaporation.

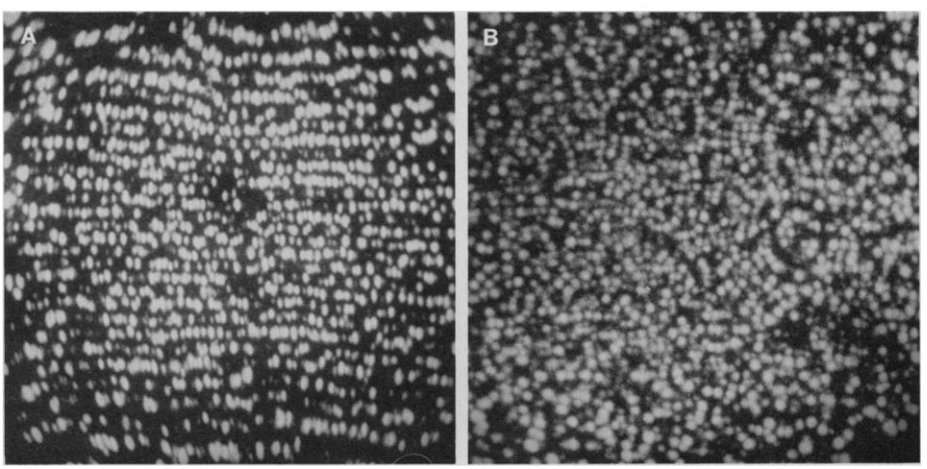

Fig. 3. FIM hydrogen ion micrographs (0.02-second exposure) at ~30 K typical of the (**A**) superconducting phase (9.2 kV) and (**B**) nonsuperconducting phase (11.6 kV).

National Bureau of Standards, Gaithersburg, MD 20899.

cated ceramic material. We chose instead to crush bulk ceramic pieces mechanically into small fragments and then to select fragments, each of which had a smooth tapered section terminating in a sharp point with approximately circular symmetry. Each selected fragment was then attached with electrically conducting epoxy to the end of a tapered tungsten wire, and the pointed fragment was imaged in the FIM in the conventional manner (*2*).

Field evaporation in the FIM produces smooth surfaces for metal and semiconductor specimens (*14*). Transmission electron microscopy of a random $YBa_2Cu_3O_{7-x}$ specimen after field evaporation and FIM imaging (Fig. 2) shows that this complex material also achieves a smoothly rounded apex shape as a result of these processes.

Field ion microscopy can be used to determine surface and bulk atomic configurations and microstructural features qualitatively (*14*); however, the extent of success is dependent on the nature of the material investigated. It is particularly relevant to the present work that both the process of field evaporation and the imaging process can depend on the atomic species, the atomic site, or both, and be sensitive to variations in local atomic geometric arrangement and electronic structure (*14*). The response to field evaporation and field ionization of $YBa_2Cu_3O_{7-x}$ cannot be predicted with the current understanding of these processes.

We have been able to image approximately 50 specimens of $YBa_2Cu_3O_{7-x}$ consistently by hydrogen ion FIM, whereas only about 60% of our attempts at neon ion FIM succeeded. Although the image quality was usually inferior in the hydrogen ion case, no qualitative features of the present images were due to chemical or to field-induced chemical effects. Most of our results were obtained with hydrogen and were confirmed by neon ion FIM. We note that in both cases some surface atoms were generally evaporating during the recording times of the FIM images. Figure 3 displays a typical hydrogen ion FIM micrograph obtained from an "as prepared" $YBa_2Cu_3O_{7-x}$ specimen and a micrograph typical of those obtained from a specimen of the "oxygen-depleted" material; both micrographs were recorded with the specimens at a temperature in the range from 25 to 40 K. (All of the FIM micrographs shown here are oriented with the orthorhombic *c*-axis upward.) The most significant difference in the micrographs is the obvious appearance of more or less parallel rows of image spots across most of the image in the superconducting "as prepared" specimen. This type of image has not been previously observed to our knowledge for a crystalline material. Figure 4 shows a neon ion FIM image of the same specimen (after considerable field evaporation) for comparison. The parallel rows are still apparent.

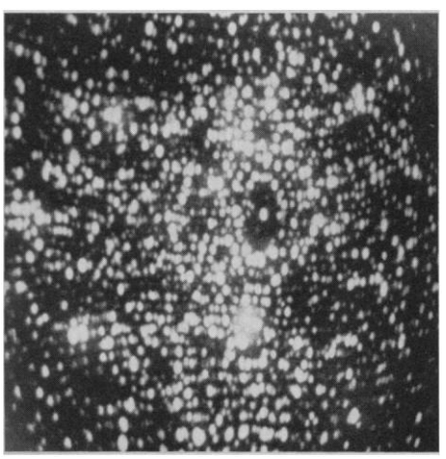

Fig. 4. FIM neon ion micrograph (13.9 kV, 0.02-second exposure) at ~30 K for the superconducting phase.

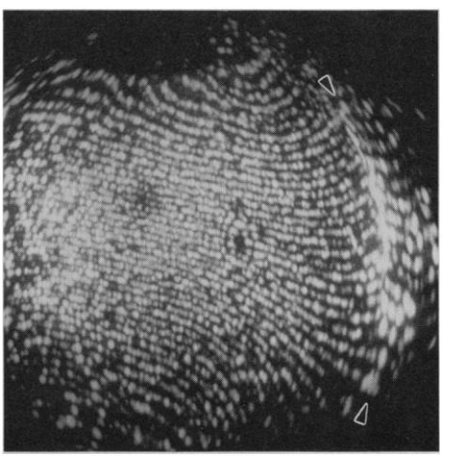

Fig. 5. FIM hydrogen ion micrograph at ~30 K (9.5 kV, 0.1-second exposure) of a superconducting $YBa_2Cu_3O_{7-x}$ with a twin boundary (indicated by arrowheads) intersecting the surface.

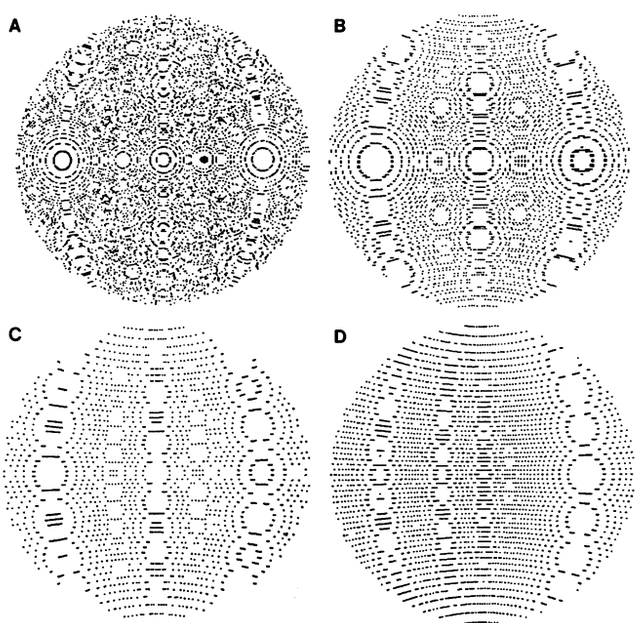

Fig. 6. Computer-simulated FIM micrographs of orthorhombic $YBa_2Cu_3O_{7-x}$ for a 35-nm radius of curvature specimen in which (**A**) all atoms, (**B**) only barium atoms, (**C**) only yttrium atoms, and (**D**) only the end plane copper and oxygen atoms are imaged. All of the simulations are stereographic (110) projections (*c*-axis upward) for atoms located within a shell of thickness 0.8 nm, except for (A), in which the shell thickness is 0.2 nm (for clarity).

The rows of image spots (Fig. 3A) are somewhat irregularly aligned, which makes row spacings difficult to define and to measure. However, in the central areas of several micrographs, spacings of some straight row sections were found to be about 1.1 to 1.4 nm apart (that is, approximately the same as the orthorhombic *c*-axis lattice parameter). Calibration of the magnifications for these measurements was done in the conventional way (*14*) and also by using an electron microscope to measure the apex radii of curvature; both methods agreed within 15%.

The appearance of rows of image spots persisted throughout field evaporation of the specimens, for depths of up to several hundred atomic layers, until the specimen ruptured or another phase was encountered. Occasionally during FIM imaging, small dim atom images were observed transiently to appear and disappear in the otherwise dark spaces between the bright rows. The depth of field evaporation was estimated with the conventional method of collapsing (field evaporating) rings of image spots, when such rings were observed; we assume that the collapse of each ring is related to the removal of one atomic plane (*14*). Thus, the imaged rows are interpreted as edge-on views of atomic or molecular layers intersecting the surface. The orientation of these layers was determined to be perpendicular to the orthorhombic *c*-axis (from the orientation of marginally visible zones of surface planes), from the orientation of observed

twin boundaries (Fig. 5), and from electron microscope observations and diffraction patterns. Electron microscopy (*3*) has shown the twin planes to be parallel (110) planes. We interpret the rows of image spots as images of atoms or molecules because they are sometimes single spots, as from a typical metal specimen, and sometimes doublet spots, as seen in FIM images of molecular species (*15*). In the present images, the doublet spots could be images of metal oxides. We associate the layer-imaging phase with the orthorhombic (superconducting) structure based on the earlier diffraction work on similar material. The other prevalent phase (Fig. 3B), which gave relatively disordered images, we associate with the nonsuperconducting tetragonal structure for similar reasons. We have found both phases in both types of material studied, but the "as prepared" samples were predominantly of the orthorhombic phase.

Since we have not yet performed atom probe mass analysis (*14*) to identify the preferentially imaging atomic or molecular species of the superconducting phase, we can only surmise, guided by computer-simulated field ion images, which atoms or molecules comprise the imaged layers. Computer simulations similar to those used in interpreting FIM images of alloys (*16*) were made to compare with the present micrographs, based on the orthorhombic unit cell of $YBa_2Cu_3O_{7-x}$ (*5*) (Fig. 6). Only those images due to the Cu-O end planes and possibly images due to only the yttrium atoms appear to be similar to the actual FIM images.

Both the superconducting and nonsuperconducting phases would be expected on the basis of atomic structure (*4, 9*) to image similarly in the FIM, unless the occurrence of superconductivity caused some selective phenomenon in the imaging process. Only the superconducting phase of $YBa_2Cu_3O_{7-x}$ appeared to field evaporate as though it was composed of layers of atoms with a relatively lower work function or higher binding energy, separated by more easily field evaporated atoms. Alternatively, the FIM image was consistent with a material composed of conducting layers separated by (nonimaging) insulating spaces. We have obtained similar results for the high T_c superconductor $YbBa_2Cu_3O_{7-x}$.

We performed experiments in which the superconducting phase was raised to about 100 K or to 300 K (both above T_c) and then re-recooled to 25 to 40 K. If no imaging was done during the time the specimen was at the higher temperatures, the preferentially imaged layers were always again seen at the low temperature. Attempts to observe a superconducting-to-normal transition by FIM, however, were not decisive (poor image quality at high temperature) due possibly to gaseous impurities in the unbaked microscope. At temperatures above T_c, the images consisted of a brightly imaging disordered array of spots and some barely discernible parallel rows. The strongly layered image, characteristic of the superconducting phase, did not always reappear when the recooling was done while continuously imaging in hydrogen. This result could be due to excessive depletion of oxygen from the specimens. Field electron microscopy (FEEM) images of the superconducting phase were observed also, but these were subject to rapid contamination in the poor vacuum ($\sim 5 \times 10^{-7}$ Pa).

We conclude that FIM and FEEM studies of the high T_c superconducting ceramics are feasible and can be used to provide detailed information about local structural and electronic properties of the various phases and their interfaces (such as phase boundaries, grain boundaries, and defects) in these fascinating materials. Although there are still some questions about the detailed interpretation of our results, the present work has provided a real space correlation between the FIM images and the occurrence of the superconducting phase in $YBa_2Cu_3O_{7-x}$ and $YbBa_2Cu_3O_{7-x}$. The observations of selectively imaging layers in the superconducting material possibly imply that the superconductivity is, in fact, inhomogeneous on an atomic scale and localized to specific layers. We tentatively identify these layers as the (Cu-O) end planes of the orthorhombic unit cell in single crystals of $YBa_2Cu_3O_{7-x}$ and $YbBa_2Cu_3O_{7-x}$.

REFERENCES AND NOTES

1. G. Bednorz and K. A. Muller, *Z. Phys.* **64**, 189 (1986); C. W. Chu *et al.*, *Phys. Rev. Lett.* **58**, 405 (1987).
2. R. Wagner, *Field-Ion Microscopy in Materials Science*, vol. 6 of Crystals Series (Springer-Verlag, Berlin, 1982).
3. G. Van Tendeloo, H. W. Zandbergen, S. Amelinckx, *Solid State Commun.* **63**, 389 (1987).
4. R. J. Cava *et al.*, *Phys. Rev. Lett.* **58**, 1676 (1987).
5. F. Beech, S. Miraglia, A. Santoro, R. S. Roth, *Phys. Rev. B* **35**, 8778 (1987).
6. T. Siegrist, S. Sunshine, D. W. Murphy, R. J. Cava, S. M. Zahurak, *ibid.*, p. 7137.
7. J. M. Tarascon, W. R. McKinnon, L. H. Greene, G. W. Hull, E. M. Vogel, *ibid.* **36**, 226 (1987).
8. J. Marcus *et al.*, *Solid State Commun.* **63**, 129 (1987).
9. M. P. Maple *et al.*, *ibid.*, p. 635.
10. A. Santoro *et al.*, *Mater. Res. Bull.* **22**, 1007 (1987).
11. Y. Hidaka, Y. Enomoto, M. Suzuki, M. Oda, J. Murakami, *Jpn. J. Appl. Phys. Part 2* **26**, L377 (1987).
12. T. R. Dinger, T. K. Worthington, W. J. Gallagher, R. L. Sandstrom, *Phys. Rev. Lett.* **58**, 2687 (1987).
13. H. Noel *et al.*, *Solid State Commun.* **63**, 915 (1987).
14. E. W. Müller and T. T. Tsong, *Field Ion Microscopy Principles and Applications* (Elsevier, New York, 1969).
15. A. J. Melmed, in *Field Ion Microscopy*, J. J. Hren and S. Ranganathan, Eds. (Plenum, New York, 1968), p. 183.
16. A. J. W. Moore, *ibid.*, p. 69.

17. We thank L. A. Bendersky for transmission electron microscopy work and J. Blendell and A. L. Johnson for providing some sample material.

29 October 1987; accepted 25 November 1987

Role of the Protein Moiety of Ribonuclease P, a Ribonucleoprotein Enzyme

CLAUDIA REICH, GARY J. OLSEN, BERNADETTE PACE, NORMAN R. PACE

The *Bacillus subtilis* ribonuclease P consists of a protein and an RNA. At high ionic strength the reaction is protein-independent; the RNA alone is capable of cleaving precursor transfer RNA, but the turnover is slow. Kinetic analyses show that high salt concentrations facilitate substrate binding in the absence of the protein, probably by decreasing the repulsion between the polyanionic enzyme and substrate RNAs, and also slow product release and enzyme turnover. It is proposed that the ribonuclease P protein, which is small and basic, provides a local pool of counter-ions that facilitates substrate binding without interfering with rapid product release.

RIBONUCLEASE P (RNASE P) removes 5′ sequences from precursor transfer RNAs (pre-tRNAs). The enzymes from the eubacteria *Escherichia coli* and *Bacillus subtilis* (*1*) are ribonucleoproteins (RNPs) consisting of an RNA (400 nucleotides) (*2, 3*) and a protein (14 kD) (*4*). Although RNase P functions in vivo as an RNP, under certain conditions the RNA alone is capable of binding and precisely cleaving tRNA precursors (*5*). We undertook a kinetic study of the RNase P reaction in *B. subtilis* to elucidate the role of the protein moiety in an RNP.

Under physiological ionic conditions, both the RNA and protein components of RNase P are required for catalysis. The

Department of Biology and Institute for Molecular and Cellular Biology, Indiana University, Bloomington, IN 47405.